Supplemental Online Material (SOM)

Carbon irradiation overcomes glioma radioresistance by eradicating stem-cells, and forming an antiangiogenic and immunopermissive niche

Sara Chiblak[1,2,†], Zili Tang[1,2,†], Dieter Lemke[1,3,†], Max Knoll[1,2], Ivana Dokic[1,2], Rolf Warta[1,4], Mahmoud Moustafa[1,2], Walter Mier[1,5], Stephan Brons[2], Carmen Rapp [1,4], Stefan Muschal[1,2], Philipp Seidel[1,2], Martin Bendzsus[1,3], Sebastian Adeberg[1,2], Otmar D. Wiestler[1], Uwe Haberkorn[1,5], Jürgen Debus[1,2], Christel Herold-Mende[4], Wolfgang Wick[1,3,§] and Amir Abdollahi[1,2,§]

[1] *German Cancer Consortium (DKTK), Heidelberg, Germany*
[2] *Division of Molecular& Translational Radiation Oncology, Heidelberg Ion Therapy Center (HIT), Heidelberg Institute of Radiation Oncology (HIRO), Heidelberg University Medical School and National Center for Tumor Diseases (NCT), German Cancer Research Center (DKFZ), Heidelberg, Germany*
[3] *Department of Neurology, Heidelberg University Medical School and National Center for Tumor Diseases (NCT), German Cancer Research Center (DKFZ), Heidelberg, Germany*
[4] *Division of Experimental Neurosurgery, Department of Neurosurgery, University of Heidelberg Medical School, Heidelberg, Germany*
[5] *Department of Nuclear Medicine, Heidelberg University Medical School and National Center for Tumor Diseases (NCT), German Cancer Research Center (DKFZ), Heidelberg, Germany*

[†] *Equal contribution*
[§] *Shared senior authors*

Supplementary Material

I. Supplementary Methods

Cells and reagents. Syngeneic spontaneous murine astrocytoma (SMA-560) cells were kindly provided by Dr. Bigner, Duke University Medical Center (Durham, NC). SMA-560, cells were cultured in DMEM Ham's F-12 (Biochrom, Berlin, Germany) supplemented with 10% FCS and 1% L-Glutamine. Gl261 glioma cells were obtained from the National Cancer Institute tumor repository (NCI-Frederick, MD). Gl261 cells were maintained in RPMI-1640 medium (Biochrom). Embryonic Stem cell-derived Microglial cells (ESdM) expressing IBa1, CD11b, CD45, F4/80, α4 integrin and β1 integrin, but not cKit and CD34 were generously donated by Dr. Harald Neumann, University of Bonn (Bonn, Germany). ESdM cells were maintained in DMEM/Ham's F-12 containing N2 supplement (Invitrogen), L-Glutamine, D-Glucose and Gentamycin. Glioma stem cells (GSC) were cultured as neurospheres using serum-free cancer stem cell medium [NCH644 and NCH441: Provitro, Berlin, Germany); T325: DMEM/F12 (Invitrogen, Darmstadt, Germany)] comprising 20% BIT (Provitro), 20 ng/ml recombinant EGF (R&D Systems, MN) and FGF (Gibco, Darmstadt, Germany). Prior to plating, cells were mechanically segregated and maintained in suspension using non-adherent tissue culture flasks (Sarstedt, Nümbrecht, Germany).

Generation of luciferase-expressing glioma cells. To generate luciferase-expressing cells, Cignal^{TM}Lenti positive control reporter (SABiosciences, CA) was transduced into cells at a multiplicity of infection of 100 under puromycin (20μg/ml) selection. After infection, luciferase activity was assessed using the Bright-Glo^{TM} luciferase Assay Kit (Promega, WI).

Coculture migration assay. SMA-560 tumor cells were plated in the lower chamber of 24 well plates and irradiated at 0Gy, 6Gy photon or 2Gy carbon ions. Microglia (ESdM) cells were seeded in 8μm pore-sized inserts (BD Biosciences, Heidelberg, Germany) and incubated with 10μM AMD3100 (Sigma-Aldrich, MO) before transferring to the irradiated plates. After 18 hours, polyethylene terephthalate (pet) membrane was stained with DAPI. Migrating ESdM cells were counted under microscope and measured by Victor X5 plate reader (PerkinElmer, MA).

Limiting dilution assay (LDA). To detect survival of KNG002, T325, and T269after irradiation, LDA was performed as described(1). Briefly, 300, 50, 8.33, and 1.33 cells were plated into 96 well plates (n=24 replicates), and irradiated with 0, 1, 2, and 4Gy photon, proton, or carbon. After three weeks of incubation, microwell plates were monitored for colony formation. Clonal frequency was calculated with the L-Calc free online software (STEMCELL Technologies, Cologne, Germany).

Long term CIR neurotoxicity. 6-8 weeks old female C57BL/6, and NcrNude mice were randomized into unirradiated, photon-irradiated and carbon-irradiated groups. Animal fixation and fractionated beam delivery were administered at doses identical to the described setups for NCH441 and Gl261 orthotopic models. Serial MRI (described below) at days 0, 45, 90, 180, and 360 post irradiation was performed.

Magnetic Resonance Imaging (MRI). T_1-weighted imaging was performed using a high resolution Spinecho sequence (TE, 600ms; TR, 14ms; field of view, 40x40; matrix, 192; voxel size, 0.2x0.2x1mm^3) five minutes after intraperitoneal administration of 80μl contrast agent Gd-DTPA Magnevist 0.5mmol/ml (Bayer Schering Pharma, Berlin, Germany). Using the Medical Imaging Interaction Toolkit (MITK, http://mitk.org), volumetry of regions of interest was determined.

Micro-Positron Emission Tomography (PET). Micro-PET was applied without tracer administration to detect secondary positrons induced by carbon irradiation and to verify irradiation accuracy in glioma-bearing mice(2). Tumor perfusion and metabolism were studied using in-house developed G^{68}-Arginie-Glycine-Aspartic acid (G^{68}-RGD) peptide-based tracer, and F^{18}-Ethyl-Tyrosine (F^{18}-FET) amino acid tracer. For bone imaging, ^{18}F-Sodium Fluoride (^{18}F-NaF) tracer was used. After

irradiation, mice were anesthetized with 2% Sevoflurane (Abbott, Wiesbaden, Germany) and placed in prone position into an Inveon small animal PET scanner (Siemens, TN). G^{68}-RGD,^{18}F-FET or ^{18}F-NaF were intravenously injected and dynamic micro-PET scans were performed as previously described (3).

I^{131}αCD133 Biodistribution. For organ distribution, NCH-644 animals treated with 0Gy, photon or carbon, as described in methods, were injected two weeks post irradiation using in-house labelled I^{131}αCD133. Mice were sacrificed after 1 hour of injection and the distributed radioactivity was measured in all dissected organs and in blood using a gamma counter. The values are expressed as percentage injected dose per gram (%Injected Dose/gram).

Expression profiling. Total RNA was isolated using TRIzol (Invitrogen) according to manufacturer's protocol. RNA integrity was determined using RNA 6000 Nano Lab on Chip kits and Agilent 2100 Bioanalyzer (Agilent, CA). RNA concentrations were determined by Nano Drop spectrophotometer (Peqlab, Erlangen, Germany). After cDNA synthesis, quantitative RT-PCR analysis was performed using TaqMan assays: **SDF1**, Assay ID: Mm00445553_m1 and Hs00171022_m1; **Hif1a**, Assay ID: Mm00468869_m1, **UBC** as endogeneous control, Assay ID: Mm01198158_m1 and Hs00824723_m1 (ABI, CA). Plates were analyzed using a 7900HT Fast Real-Time PCR System according to manufacturer's protocol.

Microarray hybridization of SMA-560 and Gl261 orthotopic models. cRNA was labeled with biotin using Encore BiotinIL Module (NuGEN, CA). For hybridization onto IIlumina mouse sentrix-8 chips (Illumina Inc, CA), biotin-labeled cRNA samples were prepared according to Illumina's recommended labeling procedure based on the modified Eberwine protocol. Hybridization was performed at 55.4°C in GEX-HCB buffer (Illumina) at a concentration of 100ng cDNA/µl and kept unsealed in a wet chamber for 20 hours. Slides were scanned with Beadstation array scanner at DKFZ genomics core facility.

Bioinformatic analysis. Generation of expression matrices, data annotation, filtering and processing were done using the TableButler software package (4). All microarray statistics were done using SUMO software. Data preprocessing was done by normalization of signals using quantile normalization algorithm without background subtraction. Arithmetic average intensities across all samples for each gene were computed. Extremely low abundant genes (average intensities<100) were excluded leaving 30,766 transcripts. Ratios were computed by dividing each individual gene by the median average for each individual gene and Log_2 transformed (virtual pool normalization). All gene expression profiles were visualized as heatmaps.

Gl261 samples were assigned to TCGA subgroups with ClaNC, a nearest centroid-based classification algorithm (5) using TCGA subtype-centroid genelist (6). To enumerate the abundance of 22-immune cell types in the tumor stroma of both SMA-560 and Gl261 murine models CIBERSORT was applied (7). Mice were not perfused prior to isolation of total RNA.

II. Supplementary References

1. Eirew P, Stingl J, and Eaves CJ. Quantitation of human mammary epithelial stem cells with in vivo regenerative properties using a subrenal capsule xenotransplantation assay. *Nature protocols.* 2010;5(12):1945-56.
2. Ammar C, Frey K, Bauer J, Melzig C, Chiblak S, Hildebrandt M, Unholtz D, Kurz C, Brons S, Debus J, et al. Comparing the biological washout of beta+-activity induced in mice brain after 12C-ion and proton irradiation. *Physics in medicine and biology.* 2014;59(23):7229-44.
3. Cheng C, Pan L, Dimitrakopoulou-Strauss A, Schafer M, Wangler C, Wangler B, Haberkorn U, and Strauss LG. Comparison between 68Ga-bombesin (68Ga-BZH3) and the cRGD tetramer 68Ga-RGD4 studies in an experimental nude rat model with a neuroendocrine pancreatic tumor cell line. *EJNMMI research.* 2011;1(34.
4. Schwager C, Wirkner U, Abdollahi A, and Huber PE. TableButler - a Windows based tool for processing large data tables generated with high-throughput methods. *BMC bioinformatics.* 2009;10(235.
5. Dabney AR. ClaNC: point-and-click software for classifying microarrays to nearest centroids. *Bioinformatics.* 2006;22(1):122-3.
6. Verhaak RG, Hoadley KA, Purdom E, Wang V, Qi Y, Wilkerson MD, Miller CR, Ding L, Golub T, Mesirov JP, et al. Integrated genomic analysis identifies clinically relevant subtypes of glioblastoma characterized by abnormalities in PDGFRA, IDH1, EGFR, and NF1. *Cancer cell.* 2010;17(1):98-110.
7. Newman AM, Liu CL, Green MR, Gentles AJ, Feng W, Xu Y, Hoang CD, Diehn M, and Alizadeh AA. Robust enumeration of cell subsets from tissue expression profiles. *Nature methods.* 2015;12(5):453-7.

Supplemental references for main text introduction section related to previously reported in-vitro studies on CIR effects in glioma.

8. Jinno-Oue A, Shimizu N, Hamada N, Wada S, Tanaka A, Shinagawa M, et al. Irradiation with carbon ion beams induces apoptosis, autophagy, and cellular senescence in a human glioma-derived cell line. International journal of radiation oncology, biology, physics. 2010;76:229-41.
9. Tomiyama A, Tachibana K, Suzuki K, Seino S, Sunayama J, Matsuda KI, et al. MEK-ERK-dependent multiple caspase activation by mitochondrial proapoptotic Bcl-2 family proteins is essential for heavy ion irradiation-induced glioma cell death. Cell death & disease. 2010;1:e60.
10. Tsuchida Y, Tsuboi K, Ohyama H, Ohno T, Nose T, Ando K. Cell death induced by high-linear-energy transfer carbon beams in human glioblastoma cell lines. Brain tumor pathology. 1998;15:71-6.

III. Supplementary Figures

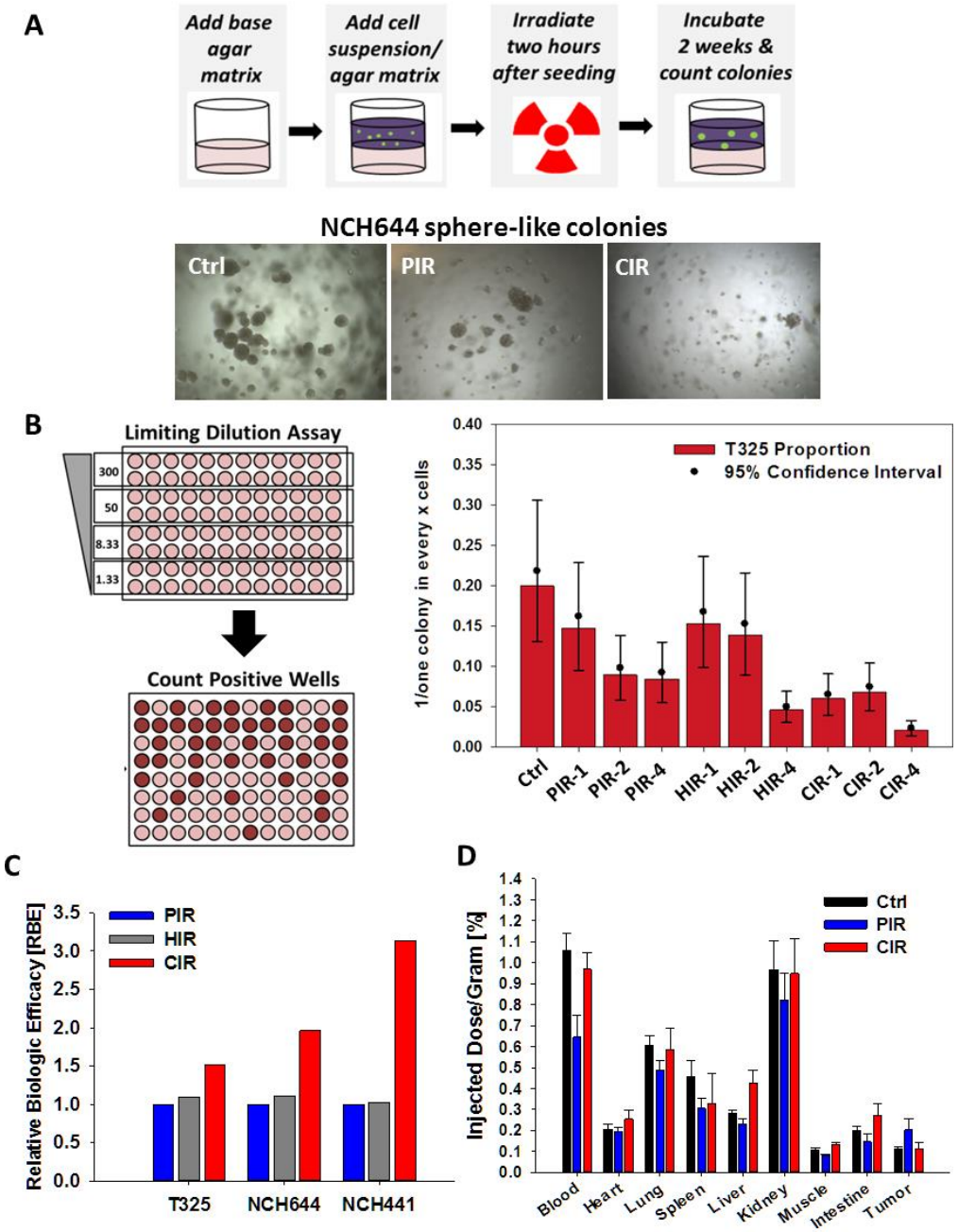

Supplementary Figure S1. CIR eradicate radioresistant Glioma Stem Cells (GSC). (A) Clonogenic survival of GSC. After mechanical dissociation of NCH644, cells were mixed in a serum-free 3D-matrix and plated onto agar precoated wells. Sphere-like colonies were counted by microscopy two weeks after irradiation. **(B) Limiting dilution assay.** Previously well characterized radioresistant human GSC, T325 cells, were seeded into wells of 96 well plates at cell dilutions accounting to 300, 50, 8.33, and 1.33 cells. Wells were monitored for colony formation after treatment with 0 (ctrl), 1, 2, and 4Gy photon (PIR), proton (HIR) or carbon irradiation (CIR). Clonogenic survival is presented as a proportion: 1 divided by the number of cells necessary to form at least one new colony (n=24 replicates). **(C)** Bar charts depicting RBE of proton (HIR) and carbon (CIR) *versus* photon (PIR) in both GSC models. **(D) I^{131}αCD133 organ distribution.** Uptake of stem cell marker, I^{131}αCD133, in murine organs and in tumor (brain) in NCH644 bearing mice two weeks post treatment (n=3 ctrl, n=5 PIR, CIR). Data are represented as % Injected Dose/gram of tissue. Error bars indicate SEM.

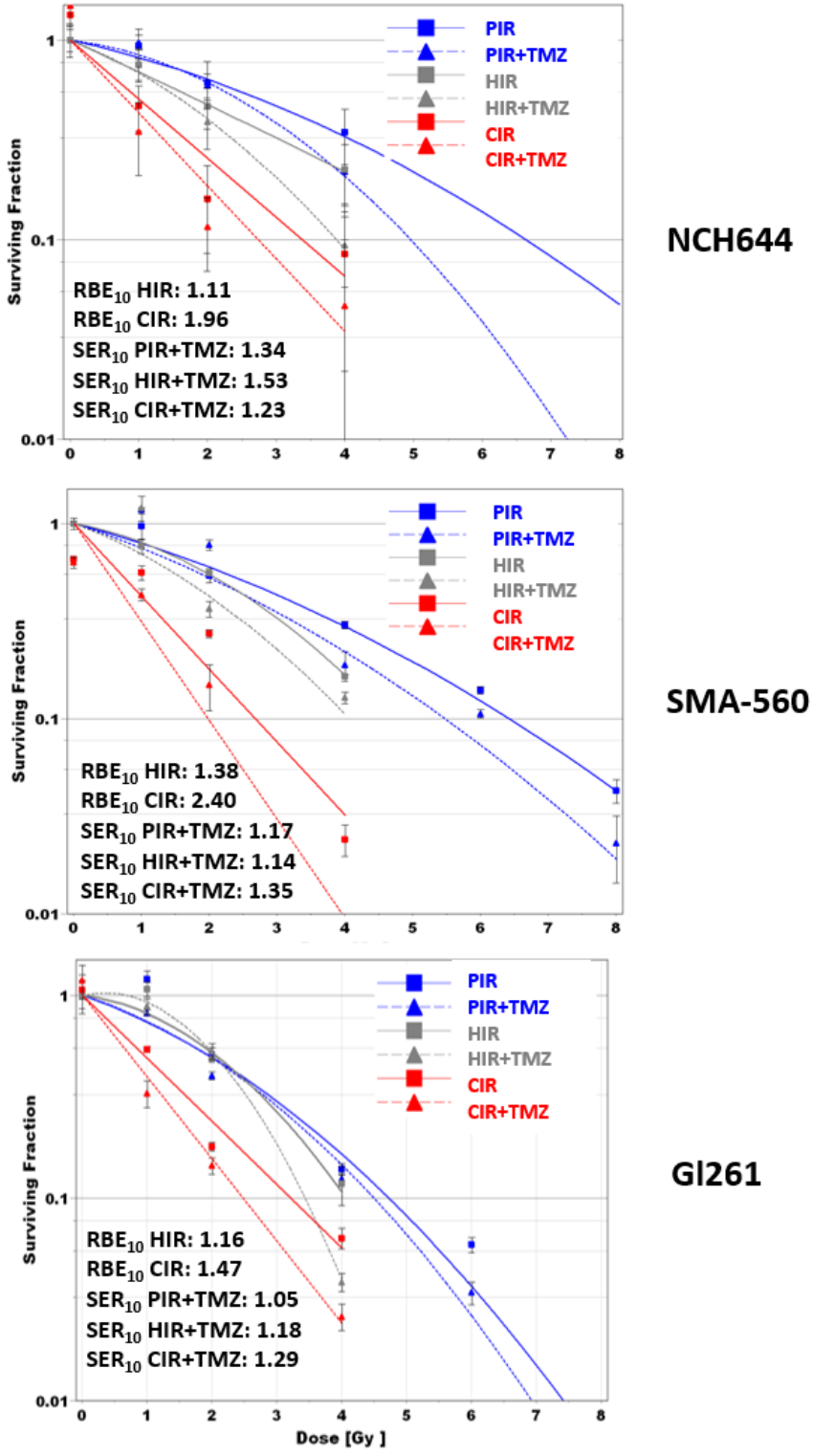

Supplementary Figure S2. In-vitro radiobiological characterization of glioma models. Clonogenic survival of NCH644 glioma stem cell culture, SMA-560 and Gl261 glioma cells was employed to assess relative biologic effectiveness (RBE) of conventional photon *versus* particle therapy (solid lines) and sensitizing enhancement ratio (SER) of temozolomide (TMZ) (dotted lines) combination in-vitro. PIR: photon irradiation, HIR: proton ion irradiation, CIR: carbon ion irradiation.

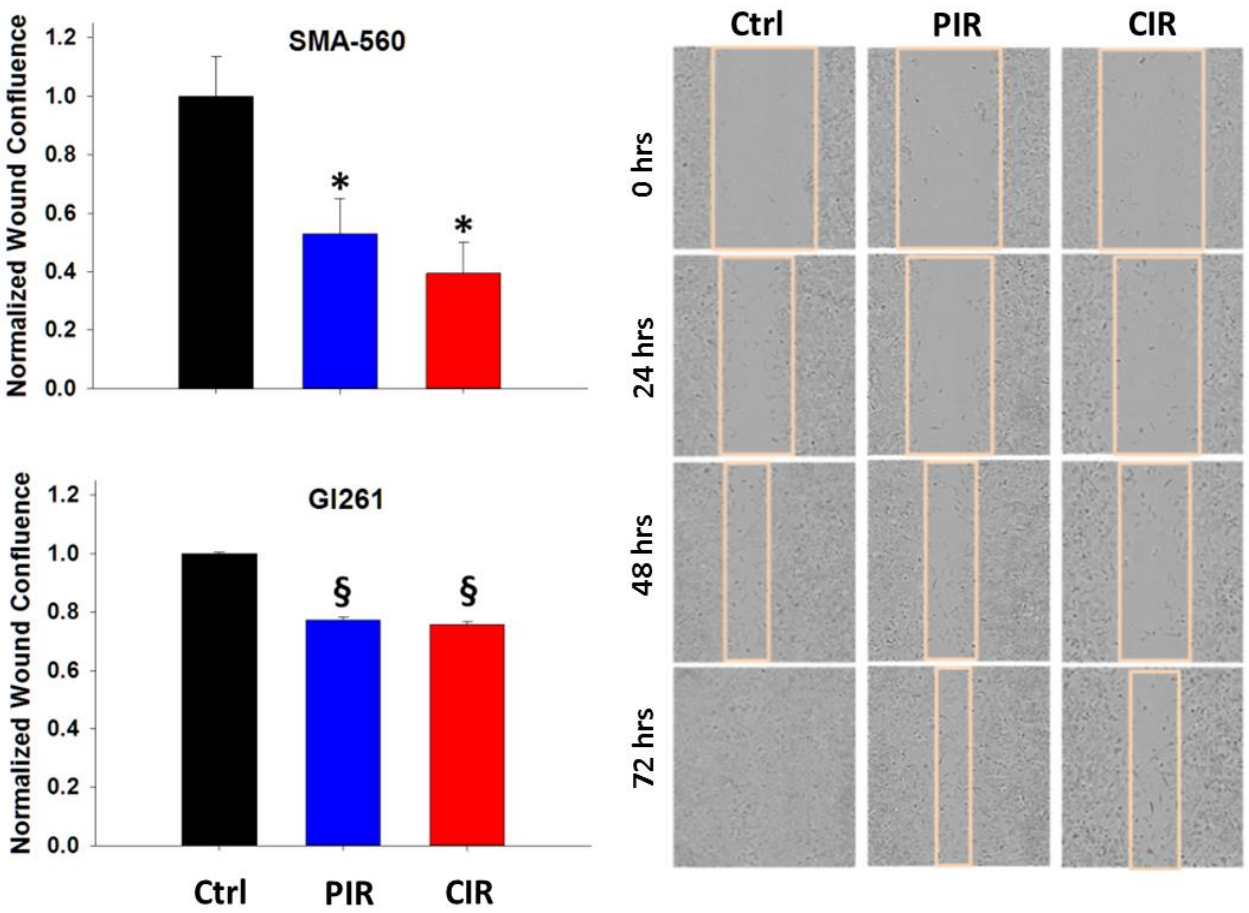

Supplementary Figure S3. Influence of irradiation on migration of glioma cells. Wound closure of SMA-560 and Gl261 scratches after irradiation with 0Gy (ctrl), 4Gy photon (PIR) or 4Gy carbon irradiation (CIR) as monitored by microscopy (Incucyte). Bars indicate mean percentage of wound confluence 72 hours post treatment. Error bars indicate SEM. *§p*<0.0001, **p*<0.05 versus control.

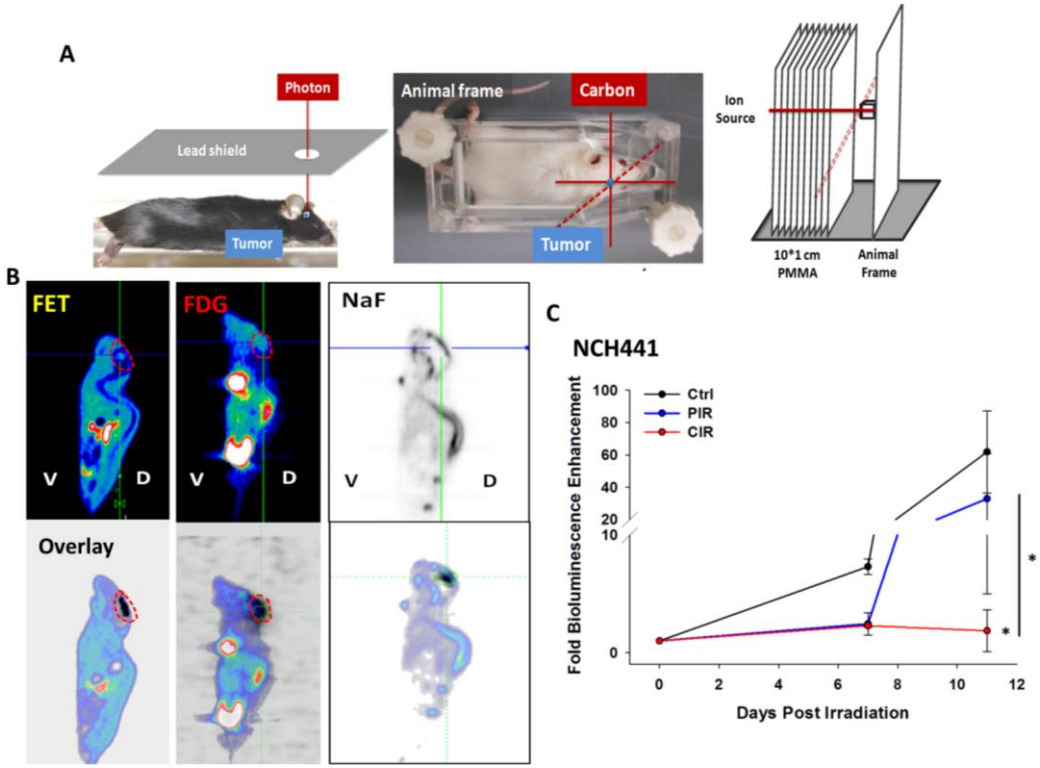

Supplementary Figure S4. High precision small animal carbon irradiation of orthotopic glioma models. (A) Fixation of mice for irradiation. Sidewise (C57Bl/6 mouse) positioning for photon irradiation. Lateral photon irradiation (via hole in lead) targeting 5x5 mm region around the cell injection site (tumor, blue) delivered by XRAD320 after protecting the rest of the body by lead shield (left panel). In contrast, custom-designed animal frame and fixation device for carbon irradiation at the right brain hemisphere of VM/DK mouse (tumor inoculation site). Target irradiation area (tumor, blue) set at the intersection of 3D laser coordinates (red lines). Beam direction (dashed line) (middle panel). For particle irradiation (proton and carbon), mice were fixed on custom-designed animal frame. The tumor region covered by SOBP (dashed line), while the tissue in plateau mimicked by transition of the beam (solid red line) through 10*1 cm Poly(methyl methacrylate) absorbers (PMMA, plexiglass) (right panel). **(B) Localization of administered dose by micro-PET imaging of carbon-induced secondary positrons (C11 PET)**. Subsequent FET-PET, FDG-PET or NaF-PET was performed. Overlay in the same animal suggested precise irradiation of the tumor-bearing hemisphere with carbon ions (in black). Target tumor area (encircled in red) is in the crossroad of the horizontal and vertical lines. **(C) Longitudinal bioluminescence of NCH441 GSC model.** Tumors were either untreated (Ctrl) or irradiated with photon (PIR) or carbon (CIR). Tumor growth was monitored longitudinally at 0, 7, and 11 days post irradiation. Fold enhancement in bioluminescence shown as line plots. *$p<0.05$ *versus* control or the indicated irradiation treatments. PET: Positron Emission Tomography, FET: Fluor^{18}-Ethyl-Tyrosine, FDG: Fluor^{18}-Desoxyglucose, NaF: Fluor^{18}-Sodium Fluoride, R: Right, L: Left, V: Ventral, D: Dorsal.

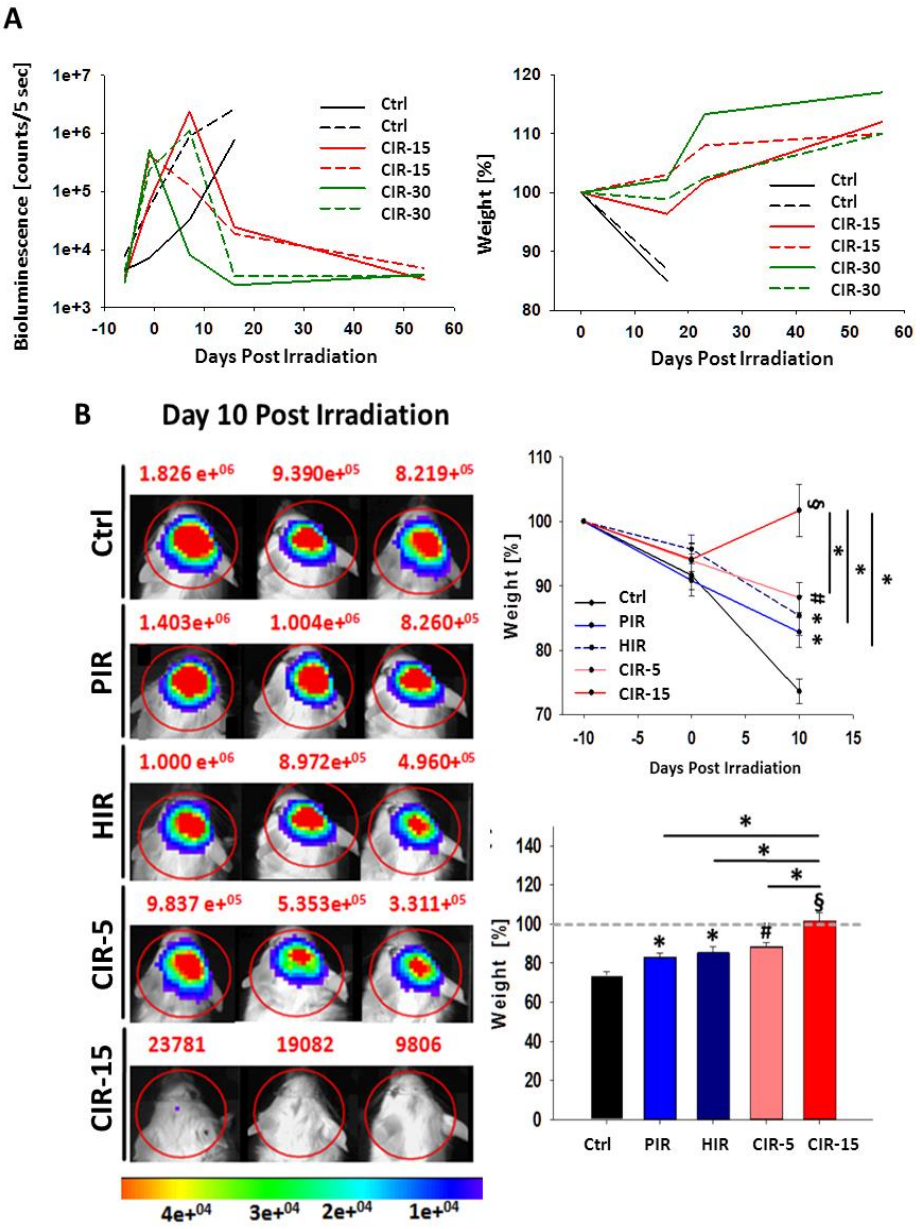

Supplementary Figure S5. Efficacy of carbon versus photon and proton irradiation in-vivo. (A) In-vivo comparison of photon, proton and carbon irradiation in an intracranial syngeneic SMA-560 murine glioma model (n=2) at 0Gy (Ctrl), 15Gy carbon (CIR-15) and 30Gy C (CIR-30) irradiation dose. Tumors were irradiated with carbon ions at day 0 and tumor growth monitored longitudinally at -6, -1, 7, 16, 26 and 54 days post irradiation. Bioluminescent signal intensities in regions of interest shown as line plots. Weight loss/gain [%] of mice was monitored. **(B)** Representative bioluminescent images, with regions of interest encircled in red, at day 10 post irradiation (n=3) SMA-560 tumors were irradiated with isodoses of 15Gy Carbon (CIR-15), photon (PIR) and proton (PIR) as well as 5Gy carbon (CIR-5). Mouse weight of SMA-560 tumor-bearing mice monitored longitudinally at all study arms. Bar charts and line plots at -2, 5 and 10 days for weight loss/gain [%] of mice post irradiation. *§p*<0.0001, *#p*<0.001, **p*<0.05 versus control or the indicated irradiation treatment.

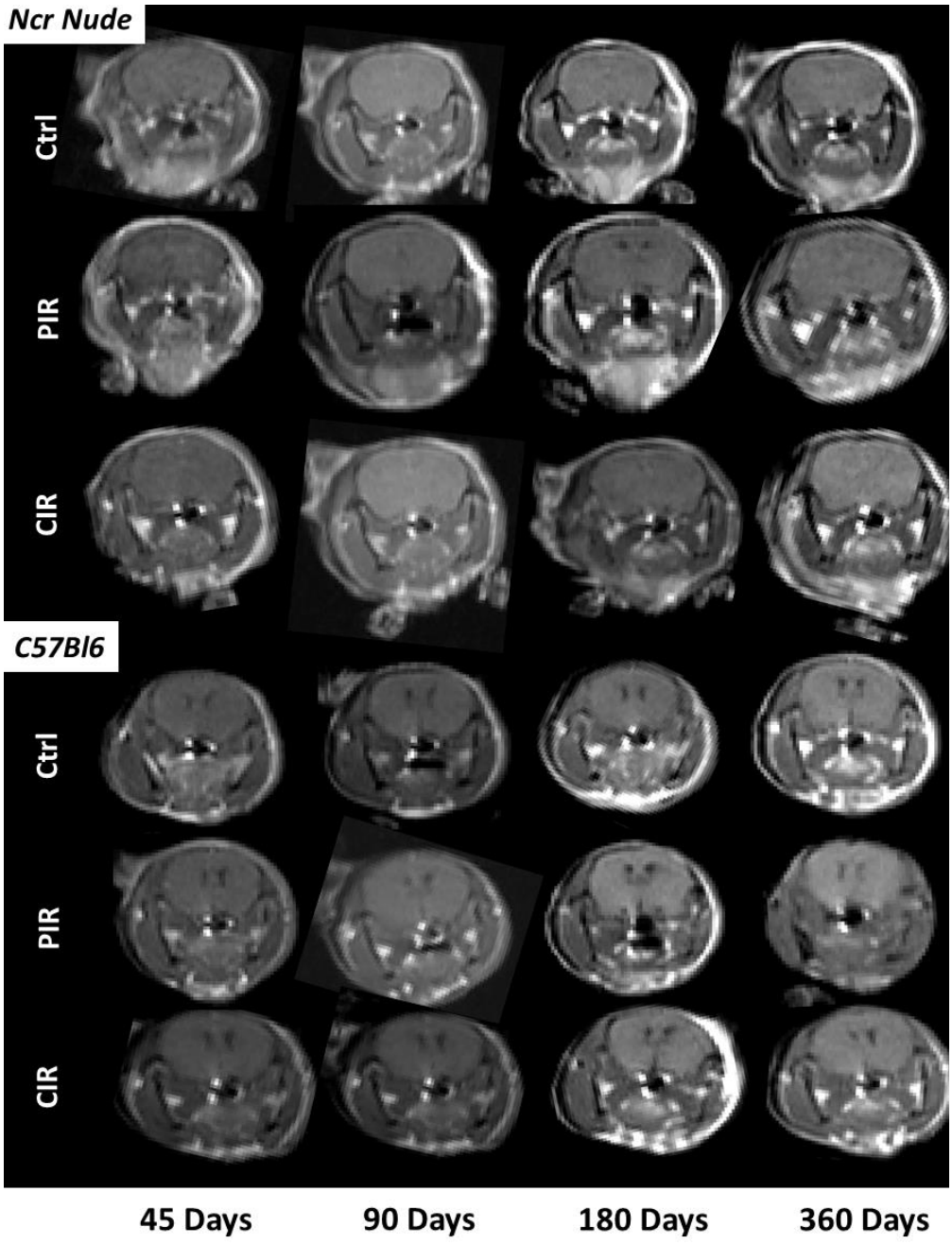

Supplementary Figure S6. Evaluation of late functional changes in mouse brain post irradiation. T1-weighted contrast-enhanced MRI images performed in the Ncr nude and C57Bl/6 mouse strains after fractionated irradiation with photon (PIR) and carbon (CIR). Serial MRI images were performed at days 45, 90, 180 and 360 days post irradiation with no apparent sign for radiation induced late effects such as enhanced temporal lobe permeability.

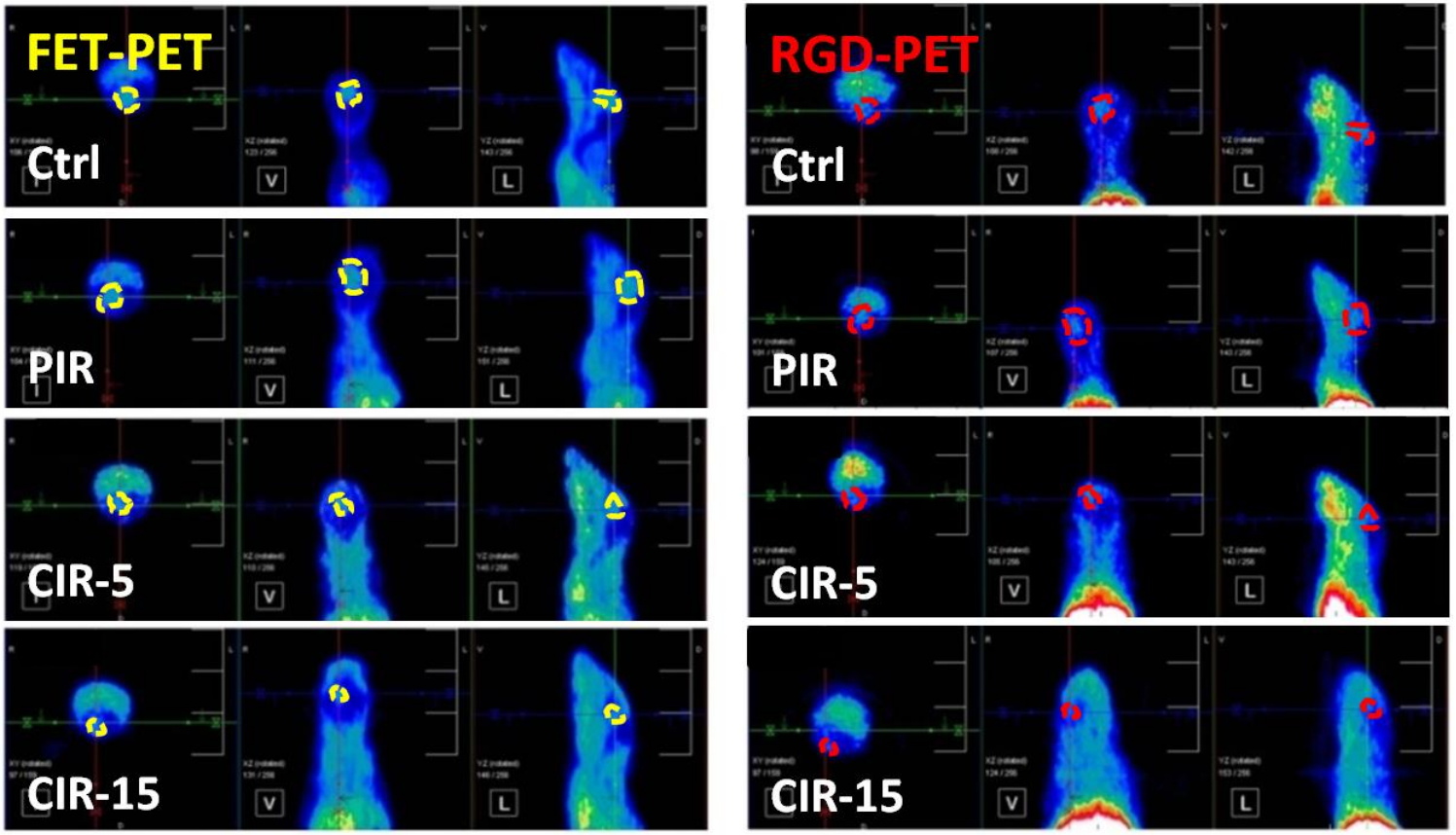

Supplementary Figure S7. Alteration of tumor vasculature and perfusion by fractionated irradiation. Representative micro-PET images of tumor perfusion (RGD-PET) and tumor metabolism (FET-PET) in SMA-560 tumors which were untreated (ctrl) or irradiated with either photon (PIR), 5Gy carbon (CIR-5) or 1Gy carbon (CIR-15). Target tumor areas encircled by dotted lines. RGD and FET intensities within indicated regions quantified and plotted in the main figure panel. PET: Positron Emission Tomography, FET: Fluor^{18}-Ethyl-Tyrosine, RGD: G^{68} Arginie-Glycine-Aspartic acid.

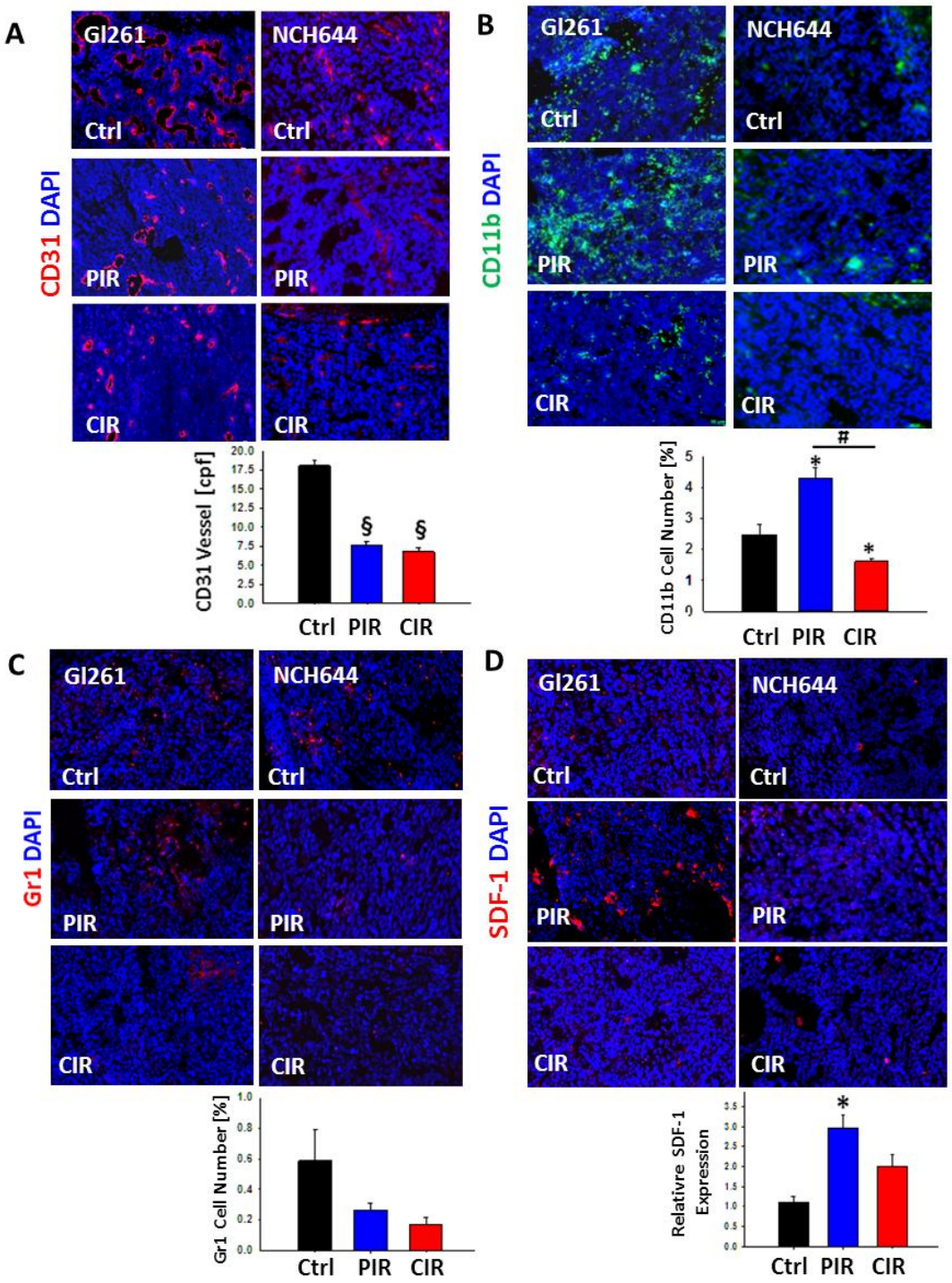

Supplementary Figure S8. Efficacy of fractionated photon versus carbon irradiation on microvasculature state, microglia and myeloid cell recruitment, as well as SDF1 expression in the Gl261 and NCH644 tumor-bearing mice. Representative photomicrographs of tumor vascular staining of anti-endothelial CD31 marker (red) **(A),** for infiltration of CD11B+ microglia (green) **(B)** and Gr1+ myeloid cells (red) **(C)** as well as SDF1 expression (red) **(D)** in the tumor stroma in all study arms. Nuclei counterstained using DAPI (blue). Bars indicate mean CD31+ positive blood vessels per field, mean CD11b and Gr1 % fluorescence intensity per field, as well as mean relative SDF1 gene expression ±SEM in the NCH644 model (n=5). *§p*<0.0001, *#p*<0.001, **p*<0.05 versus control, when shown over a bar, or *versus* the indicated irradiation treatment. Ctrl: unirradiated, PIR: photon irradiation, CIR: carbon ion irradiation.

A

Classical	Mesenchymal	Neural	Proneural	Model	Subtype	Type
379.773	570.122	703.133	628.465	GL261	Classical	Control
454.001	531.574	647.025	632.934	GL261	Classical	Control
486.140	682.168	478.017	512.080	GL261	Neural	Control
504.307	475.164	578.852	698.789	GL261	Mesenchymal	Control
464.651	580.194	562.953	619.526	GL261	Classical	Control
487.048	646.538	482.569	560.756	GL261	Neural	Carbon
479.561	599.725	515.235	600.418	GL261	Classical	Carbon
470.943	625.979	545.851	572.273	GL261	Classical	Carbon
506.404	672.122	402.295	546.729	GL261	Neural	Carbon
426.898	544.231	626.374	683.338	GL261	Classical	Carbon
477.193	631.594	512.127	575.457	GL261	Classical	Carbon
516.935	654.277	402.386	548.949	GL261	Neural	Photon
472.242	854.051	337.168	364.319	GL261	Neural	Photon
532.188	785.627	282.750	431.977	GL261	Neural	Photon
511.956	752.206	358.536	452.707	GL261	Neural	Photon
511.674	820.452	308.142	394.695	GL261	Neural	Photon

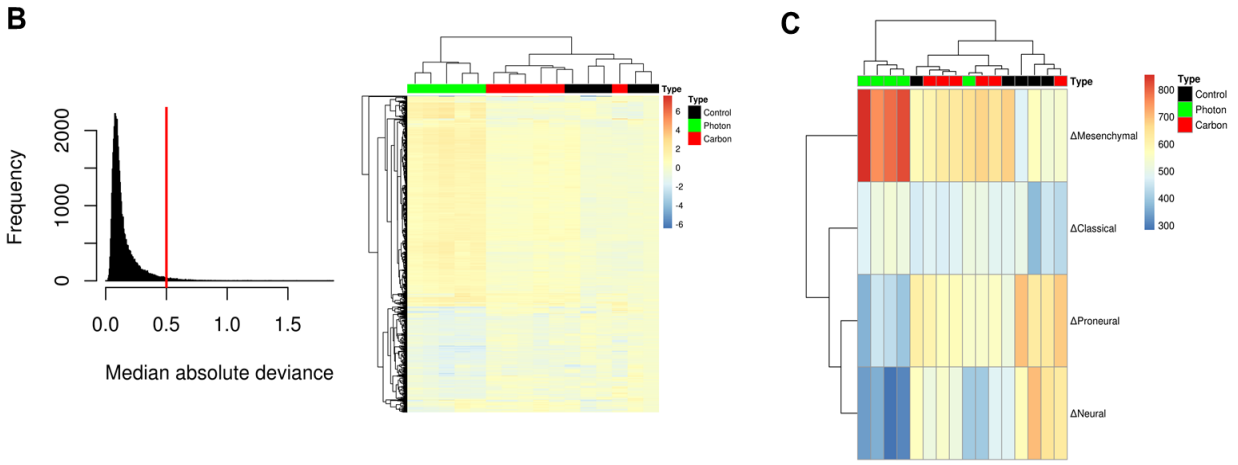

Supplementary Figure S9. Radiation-modality dependent alteration of glioblastoma subtypes (transcriptional signatures) in Gl261 cells (n=5 control, photon, n=6 carbon)**. (A)** ClaNC-derived distances of samples to treatment-relevant 840 gene-derived TCGA subgroup centroids. **(B)** Evaluation of the most variant samples by hierarchical cluster analysis (euclidean distance, complete linkage). **(C)** Hierarchical cluster analysis of differences towards centroids for all samples and all four subtypes (euclidean distance, complete linkage).

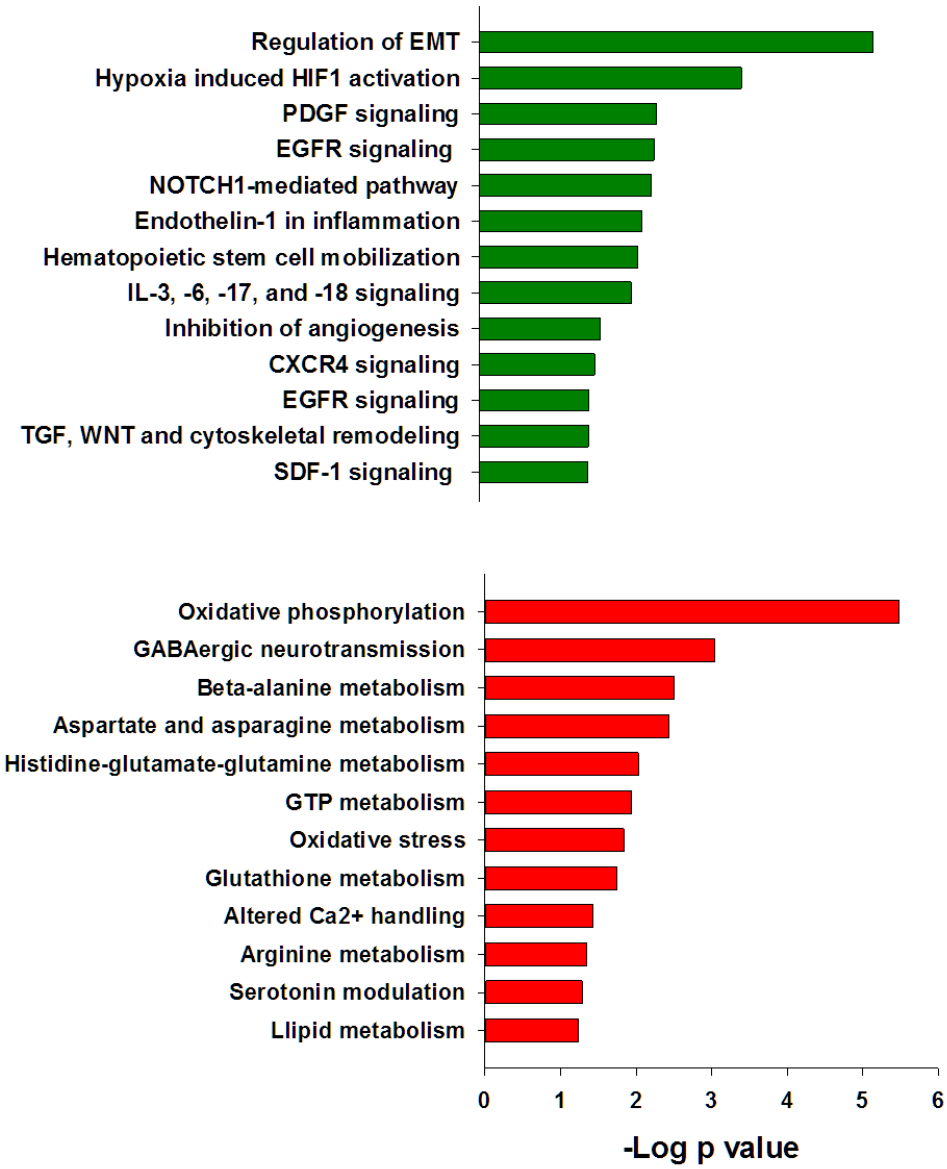

Supplementary Figure S10. Modulation of transcriptomic signatures by carbon irradiation in the SMA-560 tumor model (n=4). Using GeneGo, functional processes highly enriched with significant genes as triggered by carbon irradiation were plotted (Red=Upregulated, Green=Downregulated). Bars represent -log p-values, representing the probability for the gene ontology mapping to arise by chance.

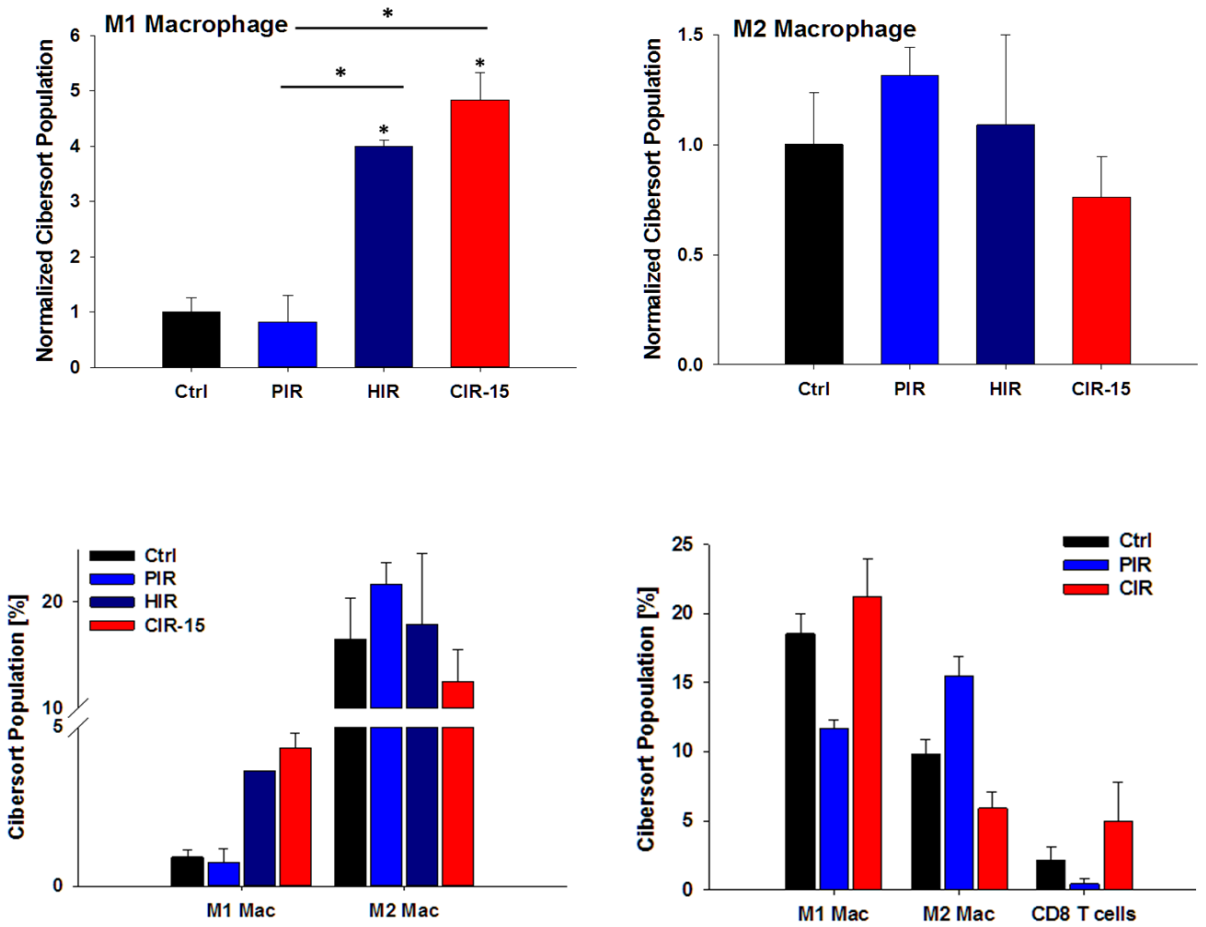

Supplementary Figure S11. **Effect of irradiation on tumor infiltrated immune cell subsets.** Enumeration of M1 and M2 macrophages in the SMA-560 tumor stroma after photon (PIR), proton (HIR) and carbon (CIR) irradiation as depicted by CIBERSORT (upper panel). Estimated absolute numbers of immune cells identified in SMA-560 (left, n=3-5/ study arm) and Gl261 (right, n=3-5/ study arm) tumor stroma at the indicated study arms (lower panel). *p<0.05 versus control or the indicated irradiation treatment

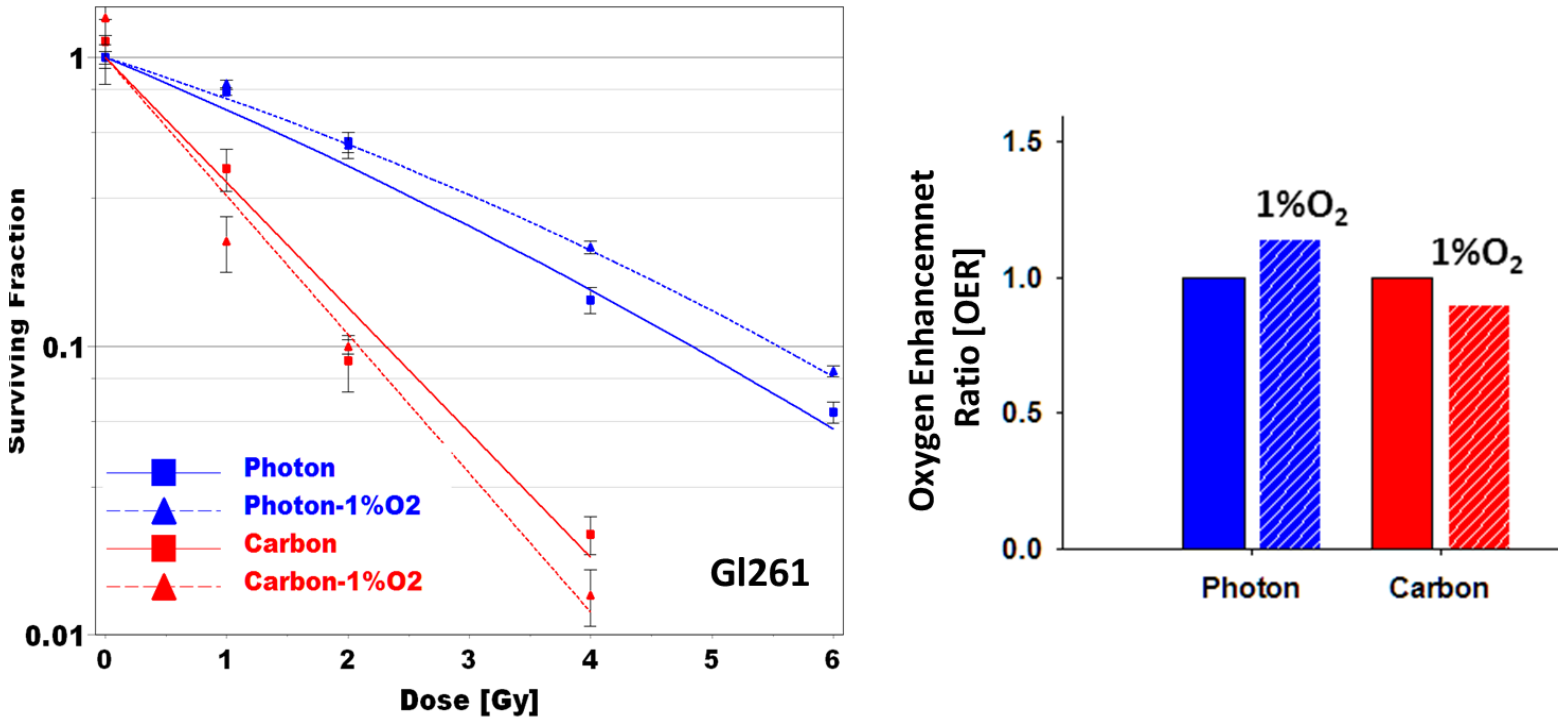

Supplementary Figure S12. Survival of Gl261 under hypoxia. Survival of Gl261 murine glioma cell line after irradiation with increasing photon and carbon doses under normoxic (solid lines) versus hypoxic (dotted lines) conditions. Bars indicate oxygen enhancement ratio (OER) for photon and carbon at both oxygen levels.

IV. Supplementary Table

Supplementary Table 1. Radiobiologic properties of human glioma stem cells (GSC) and murine glioma cell lines.

Cell line	RBE H	RBE C	SER P	SER H	SER C
Human GSC					
T325	**1.09**	**1.52**	**N/A**	**N/A**	**N/A**
NCH644	**1.11**	**1.96**	**1.34**	**1.53**	**1.23**
NCH441	**1.03**	**3.13**	**N/A**	**N/A**	**N/A**
Murine Glioma					
SMA-560	**1.38**	**2.40**	**1.17**	**1.14**	**1.35**
Gl261	**1.16**	**1.47**	**1.05**	**1.18**	**1.29**

RBE: Relative Biologic Efficacy, SER: Sensitizing Enhancement Ratio, P: photon, H: proton, C: carbon

Supplementary Table 2. Normalized tumor metabolism (FET) and perfusion (integrin, G^{68}-RGD-peptide) determined by micro-PET analysis

	FET [SUVmax]	RGD [SUVmax]
SMA-560		
Ctrl	**1 ± 0.22**	**1 ± 0.18**
PIR	**0.91 ± 0.18**	**0.83 ± 0.14**
CIR-5	**0.72 ± 0.25**	**0.48 ± 0.09**
CIR-15	**0.24 ± 0.08**	**0.14 ± 0.12**
Gl261		
Ctrl	**1 ± 0.22**	
PIR	**0.78 ± 0.15**	
CIR	**0.28 ± 0.06**	